ETH
Eidgenössische Technische Hochschule Zürich
Swiss Federal Institute of Technology Zurich

# Solid State Theory
# Solution Sheet 3

FS 2012
Prof. M. Sigrist

## Exercise 3.1 Two-orbital tight-binding model in 2d

a) The Bloch-waves constitute a basis of the (quasi-2-dimensional) Hilbert space of the system. Since the Wannier functions are the "Fourier-transforms" of the Bloch-waves, they, too, span the whole Hilbert space. Thus, we can write

$$\mathcal{H} = \sum_{\alpha,\alpha',\mathbf{j},\mathbf{j}'} \langle w_\alpha(\mathbf{r}-\mathbf{r}_\mathbf{j})|\mathcal{H}|w_{\alpha'}(\mathbf{r}-\mathbf{r}_{\mathbf{j}'})\rangle c^\dagger_{\alpha\mathbf{j}} c_{\alpha'\mathbf{j}'}, \tag{1}$$

which can be split in two terms as

$$\mathcal{H} = \sum_\alpha \mathcal{H}_\alpha + \sum_{\alpha\neq\alpha'} \mathcal{H}_{\alpha,\alpha'}. \tag{2}$$

Considering only intra-band hopping terms and restricting the sum to nearest neighbour terms, we obtain

$$\mathcal{H}_\alpha = \sum_\mathbf{j} \varepsilon_\alpha c^\dagger_{\alpha\mathbf{j}} c_{\alpha\mathbf{j}} + (t^x_\alpha c^\dagger_{\alpha(\mathbf{j}+\hat{x})} c_{\alpha\mathbf{j}} + t^y_\alpha c^\dagger_{\alpha(\mathbf{j}+\hat{y})} c_{\alpha\mathbf{j}} + \text{h.c.}) \tag{3}$$

with

$$\varepsilon_\alpha = \langle w_\alpha(\mathbf{r})|\mathcal{H}|w_\alpha(\mathbf{r})\rangle, \tag{4}$$
$$t^x_\alpha = \langle w_\alpha(\mathbf{r}-a\hat{x})|\mathcal{H}|w_\alpha(\mathbf{r})\rangle, \tag{5}$$
$$t^y_\alpha = \langle w_\alpha(\mathbf{r}-a\hat{y})|\mathcal{H}|w_\alpha(\mathbf{r})\rangle. \tag{6}$$

Considering the overlap elements $t^{x/y}_\alpha$ for both bands, we recognize that

$$t^x_{p_x} = t^y_{p_y}, \tag{7}$$
$$t^x_{p_y} = t^y_{p_x} \tag{8}$$

due to the symmetry properties of the lattice system and the atomic orbitals.

b) If we approximate the Wannier functions (which are orthogonal to each other) by atomic (hydrogen) states (which are not orthogonal to each other), we choose the orientation of the orbitals such that

$$\text{sign}(w_{p_x}(\mathbf{r})) = \begin{cases} \text{positive}, & x > 0, \\ \text{negative}, & x < 0, \end{cases} \tag{9}$$

$$\text{sign}(w_{p_y}(\mathbf{r})) = \begin{cases} \text{positive}, & y > 0, \\ \text{negative}, & y < 0. \end{cases} \tag{10}$$

Using $(\mathcal{H}_{\text{kin}} + V(\mathbf{r}))w_\alpha(\mathbf{r}) = \varepsilon_\alpha w_\alpha(\mathbf{r})$, we find for the matrix elements

$$t^x_{p_x} = \langle w_\alpha(\mathbf{r} - a\hat{x})|\varepsilon_\alpha + \sum_{\mathbf{j}\neq 0} V(\mathbf{r} - \mathbf{r_j})|w_\alpha(\mathbf{r})\rangle. \tag{11}$$

The main contribution to this matrix element comes from the region between the two lattice sites where the two orbitals have opposite sign. As $\epsilon_\alpha < 0$ and $V(\mathbf{r}) < 0$, we obtain that $t^x_{p_x} = t^y_{p_y} > 0$. For $t^y_{p_x}$, the orbitals have the same sign and $t^y_{p_x} = t^x_{p_y} < 0$. Performing the Fourier transformation

$$c_{\alpha\mathbf{j}} = \frac{1}{\sqrt{N}} \sum_{\mathbf{k}} e^{-i\mathbf{k}\cdot\mathbf{r_j}} c_{\alpha\mathbf{k}} \tag{12}$$

of the annihilation operators in the Hamiltonian, we obtain

$$\mathcal{H}_\alpha = \sum_{\mathbf{k}} \varepsilon_{\alpha,\mathbf{k}} c^\dagger_{\alpha\mathbf{k}} c_{\alpha\mathbf{k}} \tag{13}$$

with

$$\varepsilon_{p_x,\mathbf{k}} = \varepsilon + 2t_1\cos(k_x a) - 2t_2\cos(k_y a) \tag{14}$$
$$\varepsilon_{p_y,\mathbf{k}} = \varepsilon - 2t_2\cos(k_x a) + 2t_1\cos(k_y a) \tag{15}$$

where $\varepsilon = \varepsilon_{p_x} = \varepsilon_{p_y}$, $t_1 = t^x_{p_x}$, and $t_2 = -t^y_{p_x} > 0$. The band structure is visualized in Fig. 1 and the Fermi surface ($\epsilon_F = \epsilon$ for half-filling) is given in Fig. 2.

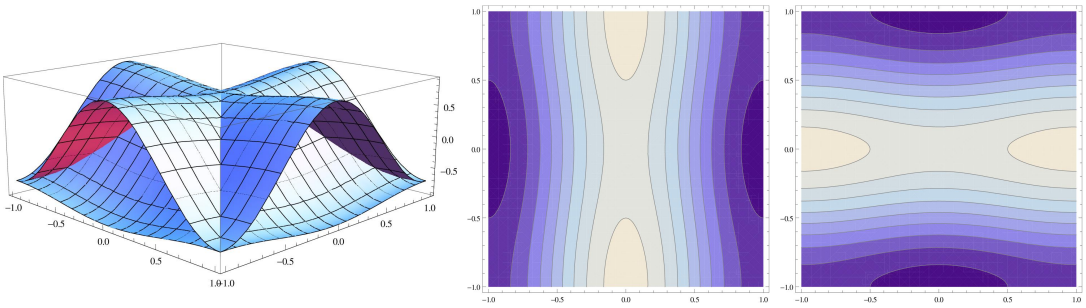

Figure 1: The band structure is visualized by a 3d plot and contour plot of the two bands ($t_1 = 0.4, t_2 = 0.05$).

c) We now also take into account the coupling between the different bands. The nearest neighbour hopping matrix elements between different bands vanishes due to the symmetry of the orbitals. Therefore, we have to consider next-nearest neighbour hopping between different bands. In the same way as before, we obtain

$$\mathcal{H}_{\alpha,\alpha'} = \sum_{\mathbf{j}} t^+_{\alpha\alpha'} c^\dagger_{\alpha(\mathbf{j}+\hat{x}+\hat{y})} c_{\alpha'\mathbf{j}} + t^-_{\alpha\alpha'} c^\dagger_{\alpha(\mathbf{j}+\hat{x}-\hat{y})} c_{\alpha'\mathbf{j}} + \text{h.c.} \tag{16}$$

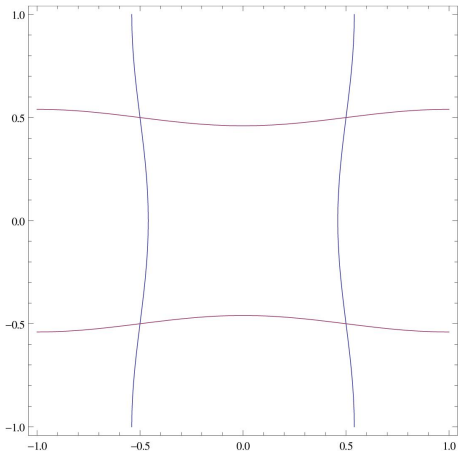


Figure 2: The Fermi surface in the absence of interband coupling ($t_1 = 0.4, t_2 = 0.05$).

with

$$t^{\pm}_{\alpha\alpha'} = \langle w_\alpha(\mathbf{r} - a(\hat{x} \pm \hat{y})|\mathcal{H}|w_{\alpha'}(\mathbf{r})\rangle \tag{17}$$

Due to symmetry properties and the analogue consideration as above, we obtain $t^{+}_{p_x p_y} = t^{+}_{p_y p_x} = -t^{-}_{p_x p_y} = -t^{-}_{p_y p_x} \equiv t_3 > 0$. Performing a Fourier transform of the Hamiltonian, we obtain

$$\mathcal{H}_{\alpha,\alpha'} = \sum_{\mathbf{k}} -4t_3 \sin(k_x a)\sin(k_y a) c^{\dagger}_{\alpha\mathbf{k}} c_{\alpha'\mathbf{k}}. \tag{18}$$

Defining $g_{\mathbf{k}} = -4t_3 \sin(k_x a)\sin(k_y a)$, the complete Hamiltonian can be written as

$$\mathcal{H} = \sum_{\mathbf{k}} \begin{pmatrix} c^{\dagger}_{p_x\mathbf{k}} \\ c^{\dagger}_{p_y\mathbf{k}} \end{pmatrix}^{\mathrm{T}} \begin{pmatrix} \varepsilon_{p_x\mathbf{k}} & g_{\mathbf{k}} \\ g_{\mathbf{k}} & \varepsilon_{p_y\mathbf{k}} \end{pmatrix} \begin{pmatrix} c_{p_x\mathbf{k}} \\ c_{p_y\mathbf{k}} \end{pmatrix} \tag{19}$$

such that to diagonalize the Hamiltonian, we have to find the Eigenvalues $E^{\pm}_{\mathbf{k}}$ of the matrix above determined by the equation

$$(\varepsilon_{p_x\mathbf{k}} - E^{\pm}_{\mathbf{k}})(\varepsilon_{p_y\mathbf{k}} - E^{\pm}_{\mathbf{k}}) - g^2_{\mathbf{k}} = 0. \tag{20}$$

The calculation is straightforwards and we obtain

$$\begin{aligned} E^{\pm}_{\mathbf{k}} = \varepsilon + (t_1 - t_2)(\cos(k_x a) + \cos(k_y a)) \\ \pm \sqrt{(t_1 + t_2)^2(\cos(k_x a) - \cos(k_y a))^2 + 16t_3^2 \sin^2(k_x a)\sin^2(k_y a)}. \end{aligned} \tag{21}$$

The resulting band structure is visualized in Fig. 3 and the Fermi surface ($\epsilon_F = \epsilon$ for half-filling) is plotted in Fig. 4.

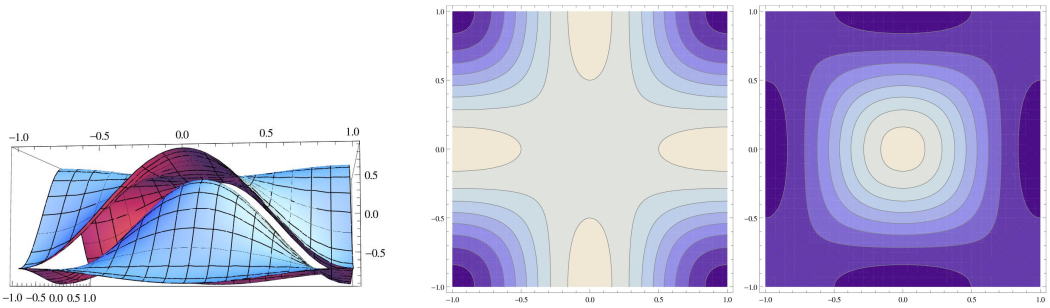

Figure 3: The band structure is visualized by a 3d plot and contour plot of the two bands ($t_1 = 0.4, t_2 = 0.05,\ t_3 = 0.1$).

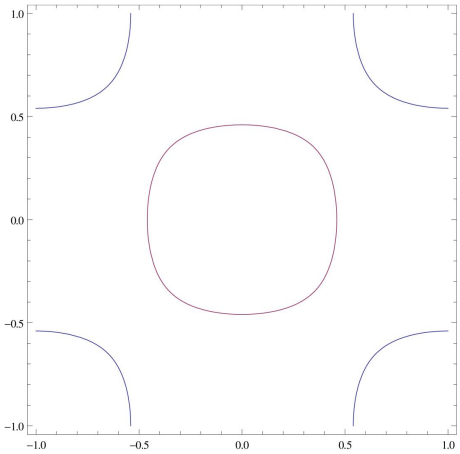

Figure 4: The Fermi surface in the presence of interband coupling ($t_1 = 0.4, t_2 = 0.05,\ t_3 = 0.1$).

### Exercise 3.2 Bloch Oscillations

a) In the presence of a uniform electric field $E$ the quasi-momentum of the wave-packet obeys

$$\hbar \dot{k} = -eE. \tag{22}$$

From the quasi-classical equations we derive immediately

$$k = -eEt/\hbar, \tag{23}$$

$$r = -\frac{2\mathrm{t}}{eE} \cos\left(\frac{aeEt}{\hbar}\right), \tag{24}$$

and see that the location of the electron indeed oscillates in time. These oscillations are caused by Bragg reflections at the Brillouin zone boundaries.

To observe these oscillations, the period of one Bloch oscillation should be less then the relaxation time. With a relaxation time of approximately $10^{-14}$ s and a lattice

constant $a \approx 1$Å, we find that the electric field would have to be at least $10^6$V/cm. With fields that strong, our approximation of only one band would break down and thus one can not see Bloch oscillations in metals.

Semiconductor superlattices, however, can have lattice constants of hundreds of Å and in addition much bigger relaxation times (of the order of $10^{-10}$s). Indeed, in such superlattices Bloch, oscillations have been observed (C. Waschke *et al.*, Phys. Rev. Lett. **70**, 3319 (1993)). Furthermore, in optical lattices, for over a decade now a playground for solid state physics, Bloch oscillations have been detected, see Fig. 5 (M. ben Dahan *et al.*, Phys. Rev. Lett. **76**, 4510 (1996)) and are still an object of interest (e.g. M. Gustavsson *et al.*, Phys. Rev. Lett. **100**, 080404 (2008) or M. Fattori *et al.*, Phys. Rev. Lett. **100**, 080405 (2008)).

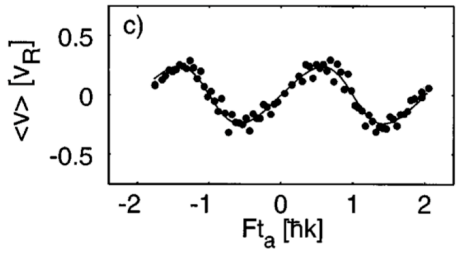


Figure 5: Experimental observation of Bloch oscillations of cesium atoms trapped in an optical lattice. From: ben Dahan *et al.* (1996).

b) The new equation for the rate of change of $k$ is

$$\hbar\dot{k} = -eE - \frac{m\dot{r}}{\tau}. \tag{25}$$

With

$$\dot{x} = -\frac{2\mathrm{t}\tau}{\hbar}\sin(q) \tag{26}$$

we thus find

$$\dot{q} = -\frac{eaE\tau}{\hbar} + \frac{2m\mathrm{t}a^2}{\hbar^2}\sin q = \alpha + \beta\sin q, \tag{27}$$

where we have changed to dimensionless variables $x = r/a$, $q = ka$ and $t' = t/\tau$. A differential equation like this can be solved analytically by a separation of variables. Note, however, that without solving this equation, we can already make some remarks about the type of solution we will obtain depending on the parameters $\alpha$ and $\beta$: For $|\alpha| > |\beta|$, there is no real $q$ that could fulfill $\alpha + \beta\sin q = 0$ and thus we do not expect the equation to have a stationary solution. Contrarily, for $|\beta| > |\alpha|$, we expect to find at least one stationary solution to the differential equation. We thus have to tackle these two cases separately:

- $|\alpha| > |\beta|$
  Performing a separation of variables, Eq. (27) can be written as

$$\frac{dq}{\alpha + \beta\sin q} = dt'. \tag{28}$$

Since $|\alpha| > |\beta|$, the left hand side has no poles and we can integrate both sides without further considerations. The right hand side yields $t' - t'_0$ and the left hand side can be calculated using the standard substitution $s = \tan(q/2)$, after which it reads

$$\int \frac{2\mathrm{d}s}{(\beta + \alpha s)^2 + (\alpha^2 - \beta^2)}. \tag{29}$$

Setting $\tilde{s} = \beta + \alpha s$ we can reduce the integral to the form

$$\int \frac{d\tilde{s}}{\tilde{s}^2 + \gamma^2}. \tag{30}$$

This is a standard integral yielding

$$t' = \frac{2}{\sqrt{\alpha^2 - \beta^2}} \arctan\left(\frac{\beta + \alpha \tan q/2}{\sqrt{\alpha^2 - \beta^2}}\right), \tag{31}$$

where we have set $t'_0 = 0$. Eventually, we find the time dependence of $q$ as

$$q(t') = 2 \arctan\left[\frac{\sqrt{\alpha^2 - \beta^2} \tan\left(t'\sqrt{\alpha^2 - \beta^2}/2\right) - \beta}{\alpha}\right]. \tag{32}$$

We see that $q$ still oscillates, however not linearly anymore, and that it is bounded to $[-\pi, \pi]$. To further analyze the situation we can calculate the velocity of the wave package $v(t) = \dot{x}(t)$ by using the quasi-classical equations of motion and the position $x(t)$ by integrating $v(t)$. The time dependence of $q$, $v$ and $x$ is shown in Fig. 6a). Obviously, a small damping does not oppress the oscillations completely but the wave-packets start drifting faster with increasing damping and the period of the oscillation increases as well.

– $|\alpha| < |\beta|$

Setting $\dot{q} = 0$ in Eq. (27) we find two $q_0$'s within $[-\pi, \pi]$ and thus two stationary solutions. To analyze whether they are stable or not we expand $q$ around the stationary solution $q = q_0 + \delta q$ and linearize the equation of motion

$$\dot{q_0} + \delta\dot{q} = \delta\dot{q} = \alpha + \beta \sin q_0 + \beta \cos q_0 \delta q = \beta \cos q_0 \delta q. \tag{33}$$

Figure 7 shows that the cosines of the solutions $q_0$ and $q'_0 = \pi - q_0$ have always opposite sign and the tangents at these points opposite slope, respectively. Thus, we always find an 'attractive' and a 'repulsive' $q_0$, meaning a stable and an unstable stationary solution. We also realize that we have to take some more care performing the integration as now we have two poles between which we can integrate (Note that we actually have two intervals between which we can integrate depending on the boundary conditions due to the periodicity of $q$!). We thus anticipate two different solutions. We can start from Eq. (29) by slightly rewriting it as

$$\int \frac{2\mathrm{d}s}{(\beta + \alpha s)^2 - (\beta^2 - \alpha^2)} \tag{34}$$

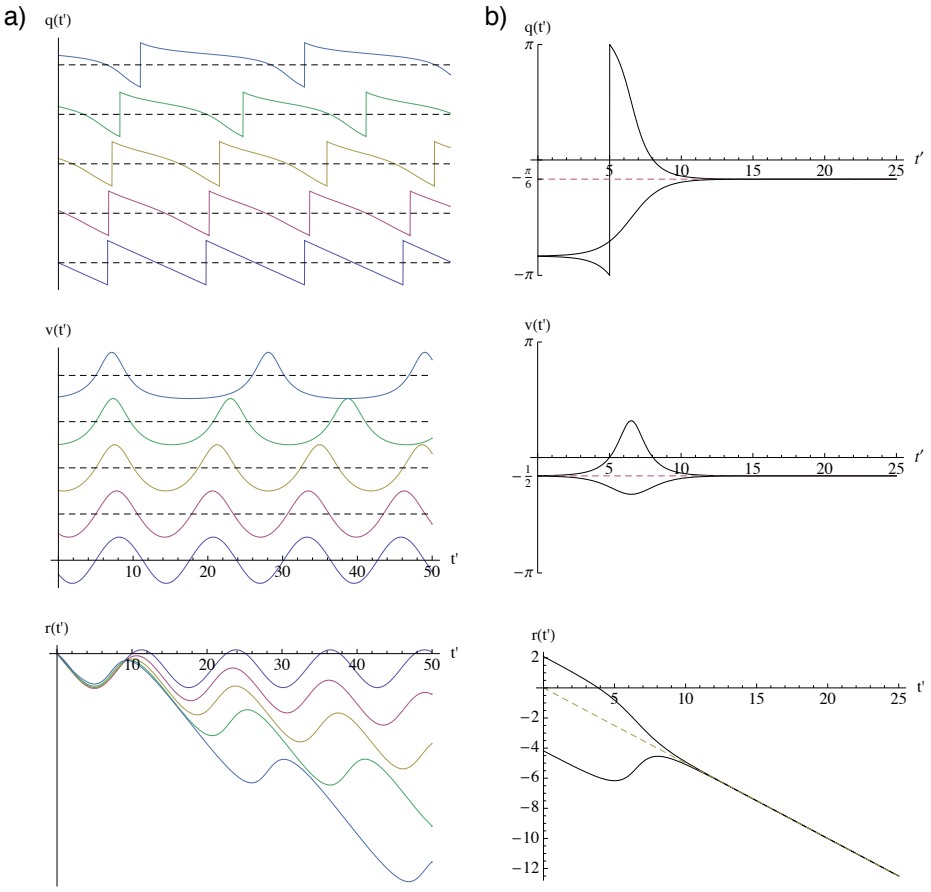


Figure 6: The time evolution for the quasi-momentum $q$, the velocity $v$ and the position $r$ for the slightly damped and the overdamped case. For all plots, $\alpha = -0.5$. a) The plots show $q$, $v = \sin q$ and $r$ for $\beta = 0, -0.1, -0.2, -0.3$ and $-0.4$. The curves in the $q$- and $v$-plots are shifted for better visibility. While for $\beta = 0$ we have the expected oscillation around a fixed point, for $0 < |\beta| < |\alpha|$ the wave packet starts to drift with an increasing velocity, yet still oscillating with an increasing period. b) $\beta = -1$: Shown are the two different ways for $q$ to converge to the stable stationary solution $q = -\arcsin 1/2$.

and find immediately

$$t' = \frac{1}{\sqrt{\beta^2 - \alpha^2}} \ln \left| \frac{\beta + \alpha \tan q/2 - \sqrt{\beta^2 - \alpha^2}}{\beta + \alpha \tan q/2 + \sqrt{\beta^2 - \alpha^2}} \right| . \tag{35}$$

Indeed, we find that we have to differentiate between two cases depending on the relative sign of the numerator and the denominator in the log.
If the signs are equal, the solution for $q(t')$ reads

$$q(t') = 2 \arctan \left[ - \frac{\sqrt{\beta^2 - \alpha^2} \coth \left( t' \sqrt{\beta^2 - \alpha^2}/2 \right) + \beta}{\alpha} \right] , \tag{36}$$

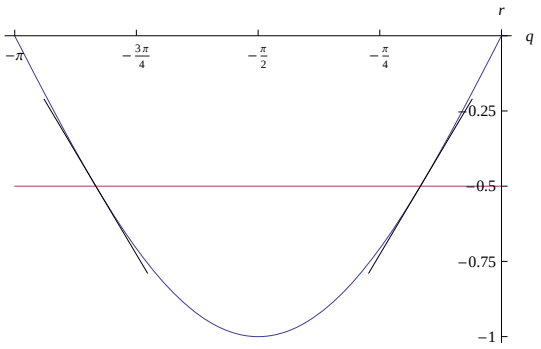


Figure 7: To emphasize the two different stationary solutions the graphical solution of Eq. (27) is plotted. We see that the slope of the tangents is always opposite for the two solutions, resulting in a stable and an unstable stationary solution.

a solution we would not simply have obtained by setting $|\beta| > |\alpha|$ in Eq. (32). We see here clearly that $q(t')$ becomes constant for $t' \to \infty$ and it can be shown easily that it converges towards $q \to q_0$. Additionally, one can easily reassure oneself that the relative sign of the denominator and the numerator in the log in Eq. (35) remains positive and the solution is consistent. Figure 6b) shows plots of $q$, $v$ and $x$ for the two different cases of intervals. Depending on the boundary conditions, the wave-packet moves always in the same direction or performs one single wiggle.

If the signs are different, the solution for $q(t')$ reads

$$q(t') = 2\arctan\left[-\frac{\sqrt{\beta^2-\alpha^2}\tanh\left(t'\sqrt{\beta^2-\alpha^2}/2\right)+\beta}{\alpha}\right]. \tag{37}$$

Summarizing, we have found that, depending on the applied field $E$ and the relaxation time $\tau$, we can either have oscillating electrons drifting slightly or electrons only drifting. The condition separating these two cases is

$$|E| < \frac{2m\mathrm{ta}}{e\hbar\tau}. \tag{38}$$

We can also analyze the stationary situation for $t' \to \infty$ some more. As in that case $\dot{q} = 0$,

$$\frac{m\dot{r}}{\tau} = -eE. \tag{39}$$

Since the current in the metal is given by $j = -en\dot{r}$ with $n$ the density of electrons we find for the conductivity

$$\sigma = \frac{e^2 n\tau}{m}, \tag{40}$$

the famous Drude form.

For further information on Bloch oscillations, the article by J.B. Kireger and G.J. Iafrate in Physical Review B **33**, 5494(1986) is recommended.